Online Supporting Material:
Model Formulations and Numerical Methods

Ting Ye[1], Nhan Phan-Thien, Boo Cheong Khoo and Chwee Teck Lim

1 Model formulations

1.1 Dissipative particle dynamics

Dissipative particle dynamics (DPD) is a mesoscale stochastic simulation method proposed by Hoogerbrugge and Koelman (1), and reformulated by Español and Warren (2) to ensure a thermal equilibrium state. It is widely applied to simulate complex fluid systems, such as multiphase flow, colloidal suspensions, and polymeric blends. In a DPD system, the simulation domain is represented by a system of particles, called DPD particles, and the interaction between any two particles is characterized by the DPD force ($\mathbf{f}_{ij}^{DPD}$), which consists of a conservative ($\mathbf{f}_{ij}^{C}$), a dissipative ($\mathbf{f}_{ij}^{D}$) and a random ($\mathbf{f}_{ij}^{R}$) forces,

$$\mathbf{f}_{ij}^{DPD} = \mathbf{f}_{ij}^{C} + \mathbf{f}_{ij}^{D} + \mathbf{f}_{ij}^{R}. \tag{1}$$

The conservative force is related to the compressibility of fluid, and the dissipative force mainly determines the viscosity of fluid. The balance between the random and the dissipative forces maintains a constant temperature (specific kinetic energy) in the system. They are defined as (2)

$$\mathbf{f}_{ij}^{C} = \alpha_{ij}\omega^{C}(r_{ij})\hat{\mathbf{r}}_{ij}, \tag{2}$$

$$\mathbf{f}_{ij}^{D} = -\gamma_{ij}\omega^{D}(r_{ij})(\vec{\mathbf{r}}_{ij}\cdot\mathbf{v}_{ij})\hat{\mathbf{r}}_{ij}, \tag{3}$$

$$\mathbf{f}_{ij}^{R} = \sigma_{ij}\omega^{R}(r_{ij})\,\xi_{ij}\big/\sqrt{dt}\,\hat{\mathbf{r}}_{ij}, \tag{4}$$

where α_{ij}, γ_{ij} and σ_{ij} are coefficients to characterize the force strengths; ξ_{ij} is a normally distributed random variable with zero mean and unit variance; dt is the time step (in the context of stochastic differential equation); $\omega^{C}(r_{ij})$, $\omega^{D}(r_{ij})$ and $\omega^{R}(r_{ij})$ are weight functions; $\mathbf{r}_{ij} = \mathbf{r}_i - \mathbf{r}_j$, $r_{ij} = \left|\mathbf{r}_{ij}\right|$, $\hat{\mathbf{r}}_{ij} = \mathbf{r}_{ij}/r_{ij}$, and $\mathbf{v}_{ij} = \mathbf{v}_i - \mathbf{v}_j$. The weight functions $\omega^{C}(r_{ij})$ and $\omega^{D}(r_{ij})$ are defined by

[1] Department of Mechanical Engineering, National University of Singapore, Singapore 117576

$$\omega^C(r_{ij}) = \begin{cases} \left(1 - r_{ij}/r_c\right), & r_{ij} < r_c \\ 0, & r_{ij} \geq r_c \end{cases}, \tag{5}$$

$$\omega^D(r_{ij}) = \begin{cases} \left(1 - r_{ij}/r_c\right)^s, & r_{ij} < r_c \\ 0, & r_{ij} \geq r_c \end{cases}, \tag{6}$$

where r_c is the cut-off radius; s is the exponent of the dissipative weight function. The weight function $\omega^R(r_{ij})$ satisfies

$$\omega^D(r_{ij}) = \left[\omega^R(r_{ij})\right]^2, \tag{7}$$

to keep a constant Boltzmann temperature $k_B T$ in the DPD system:

$$\sigma_{ij}^2 = 2k_B T\gamma_{ij}\,. \tag{8}$$

1.2 Discrete cell model

In the present discrete cell model, the whole cell is discretized into a system of DPD particles; the particles on the cell surface are connected into a viscoelastic triangular network representing the cell membrane. Hence, the membrane force $\mathbf{f}_i^M$ acting on the i^{th} particle consists of the elastic ($\mathbf{f}_i^{Ela}$) and viscous ($\mathbf{f}_i^{Vis}$) parts,

$$\mathbf{f}_i^M = \mathbf{f}_i^{Ela} + \mathbf{f}_i^{Vis}. \tag{9}$$

The elastic part is characterized by a total energy potential U_{total}, (3)

$$\mathbf{f}_i^{Ela} = \frac{\partial U_{total}}{\partial \mathbf{r}_i}, \tag{10}$$

where

$$U_{total} = U_{in-plane} + U_{bending} + U_{area} + U_{volume}, \tag{11}$$

in which $U_{in-plane}$ is the in-plane energy for describing the stretching deformation, $U_{bending}$ the bending energy for the bending deformation, U_{area} the area-constraint energy for the area conservation, and U_{volume} the volume-constraint energy for the volume conservation. In the present

work, the membrane particles are connected by nonlinear-worm like chains, and therefore the in-plane energy is defined as (4)

$$U_{in-plane} = \sum_{j=1}^{N_c} \left(\frac{k_B T l_j^{max}}{4 p_j} \frac{3 s_j^2 - 2 s_j^3}{1 - s_j} + \frac{k_j}{l_j} \right), s_j = \frac{l_j}{l_j^{max}}, \tag{12}$$

where l_j and l_j^{max} are the current and maximum length of the j^{th} chain; $k_B T$ is the Boltzmann temperature; p_j is the persistence length; and k_j is a coefficient; N_c is the number of chains. It should be pointed out that the first part in Eq. (12) is attractive, but the second part repulsive to maintain a nonzero equilibrium length of each chain. The bending energy provides resistance to membrane wrinkle and distortion, (5) defined as

$$U_{bending} = \sum_{j=1}^{N_c} k_b \left(1 - cos\left(\theta_j - \theta_j^R \right) \right), \tag{13}$$

where k_b is the bending coefficient; θ_j is the instantaneous angle between two adjacent triangles having the common j^{th} edge; θ_j^R is the spontaneous angle. The area conservation constraint is given by

$$U_{area} = \frac{k_{ga} (A_{tot} - A_{tot}^{des})^2}{2 A_{tot}^{des}} + \sum_{j=1}^{N_t} \frac{k_{la} (A_j - A_j^{des})^2}{2 A_j^{des}}, \tag{14}$$

where k_{ga} and k_{la} are the global and local area constraint constants; A_{tot} and A_j are the areas of the cell membrane and j^{th} triangle; A_{tot}^{des} and A_j^{des} are the corresponding desired areas; N_t is the number of triangles on the cell membrane. The first part in Eq. (14) places a constraint on the global area of cell membrane, while the second part on the global area of each triangle. Note that the conservation of surface area is achieved by increasing total and local area constraint constants. Similarly, the volume conservation constraint is

$$U_{volume} = \frac{k_v (V_{tot} - V_{tot}^{des})^2}{2 V_{tot}^{des}}, \tag{15}$$

where k_v is the global volume constraint constant, V_{tot} and V_{tot}^{des} are the current and desired global volumes of the cell.

The viscous part in Eq. (9) is modelled by the general fluid particle model, (6) in which a viscous component is introduced into each membrane chain,

$$\mathbf{f}_i^{Vis} = \sum_{\substack{j \\ (i,j)\in N_c}} (\mathbf{f}_{ij}^{D,Vis} + \mathbf{f}_{ij}^{R,Vis}), \tag{16}$$

where the subscripts i and j are the two endpoints of a chain; $\mathbf{f}_{ij}^{D,Vis}$ is the dissipative part mainly determined the viscosity of cell membrane, (6)

$$\mathbf{f}_{ij}^{D,Vis} = -\gamma^T \mathbf{v}_{ij} - \gamma^C (\mathbf{v}_{ij} \cdot \hat{\mathbf{r}}_{ij}) \hat{\mathbf{r}}_{ij}, \tag{17}$$

where γ^T and γ^C are the dissipative parameters. In addition, a random part $\mathbf{f}_{ij}^{R,Vis}$ is added in Eq. (16) to balance the temperature via a fluctuation-dissipation theorem (6),

$$\mathbf{f}_{ij}^{R,Vis} = \sqrt{2k_B T}\left(\sqrt{2\gamma^T}\,\overline{d\mathbf{W}_{ij}^S} + \frac{\sqrt{3\gamma^C - \gamma^T}}{3} tr[d\mathbf{W}_{ij}]\mathbf{I}\right) \cdot \hat{\mathbf{r}}_{ij}, \tag{18}$$

where $\mathbf{I}$ is the unit second-order tensor; $tr[d\mathbf{W}_{ij}]$ is the trace of a random matrix formed by independent Wiener increments $d\mathbf{W}_{ij}$; $\overline{d\mathbf{W}_{ij}^S}$ is the traceless symmetric part of $d\mathbf{W}_{ij}$.

Fedosov et al. (3) conducted a linear analysis for a regular hexagonal network on the cell membrane, and derived the macroscopic shear modulus η^M as

$$\eta^M = \frac{\sqrt{3}k_B T}{4 p_j l_{j,0}}\left[\frac{s_0}{2(1-s_0)^3} - \frac{1}{4(1-s_0)^2} + \frac{1}{4}\right] + \frac{3\sqrt{3}k_j}{4 l_{j,0}^3}, \; s_0 = \frac{l_{j,0}}{l_j^{max}}, \tag{19}$$

where the subscript '0' refers to the stress-free state. The bending modulus κ^M is shown to be (3)

$$\kappa^M = \frac{2}{\sqrt{3}} k_b, \tag{20}$$

and the area dilution modulus ζ^M as (3)

$$\zeta^M = 2\eta^M + k_{ga} + k_{la}. \tag{21}$$

The membrane viscosity is estimated as (3)

$$\mu^M = \sqrt{3}\gamma^T + \frac{\sqrt{3}\gamma^C}{4}. \tag{22}$$

2 Numerical methods

At the initial state, the particle velocity is set by

$$\boldsymbol{v}_i = \sqrt{3\left(1-\frac{1}{N-N_w}\right)\frac{T}{m_i}}\boldsymbol{e}_i\,, \tag{23}$$

where N and N_w are the numbers of total particles and wall particles; $\boldsymbol{e}_i$ is a unit random vector. This velocity ensures that the initial system temperature is T. The particle acceleration is set to be zero. As a result, the DPD force $\mathbf{f}_{ij}^{DPD}$ and the viscous part $\mathbf{f}_i^{Vis}$ of membrane force are easily calculated. On the other hand, the initial state of cell is regarded as a stress-free state, such that the desired area (A_j^{des} and A_{tot}^{des}) and volume (V_{tot}^{des}) are set to be the values of initial area and volume of cell, as well as the equilibrium length $l_{j,0}$ and spontaneous angle θ_j^R. Therefore, the elastic part of membrane force is also obtained. Subsequently, we use the modified velocity-Verlet algorithm (7) to solve the equation governing the particle motion, such that the location and velocity of each particle is updated.

3 Dynamics in shear flow

It has been shown that the cell models with and without included parasites can produce a reasonable stretching deformation and shape relaxation time for healthy and malaria-infected RBCs. In this section, we further study their dynamic behaviours in simple shear flow. Models with included parasites are much more complex to be implemented in numerical simulations of simple shear flow, because the rotation of rigid parasites should be considered. Therefore, numerical works on the malaria-infect RBC often adopted models without included parasites, such as Suresh et al.'s work (8, 9), and Fedosov et al.'s work (10). Here, we also use the cell model without included parasite. The dynamical motions of a cell in shear flow are broadly classified into three types (11): tank-treading, swinging, and tumbling. However, Yazdani and Bagchi (12) pointed out that the swinging motion is more complex, and classified it into several types: swinging with tank-treading, breathing at zero inclination, breathing with swinging, and breathing with tumbling. We use this detailed classification to identify our simulation results shown in Fig. 1. At the same shear rate, hRBC and iRBC exhibit the different dynamical behaviours. The hRBC first inclines and gradually approaches to a steady state, known as the tank-treading motion, consistent with Yazdani et al.'s work (12). In this motion, the initial biconcave dimples are completely absent; both the deformed shape and its angle of inclination undergo some slight periodic oscillations. The rRBC exhibits a similar behaviour to the hRBC, but the

biconcave dimples are not completely absent and the oscillations are obvious. This mode is called swinging with tank-treading motion (12). The tRBC undergoes a complex shape deformation, where the membrane folds toward the cell interior so as to form two concave cusp-like dimples at the tRBC ends. The folding is periodic, and the tRBC swings with a periodic angular oscillation. This behaviour is called breathing with swinging motion (12). The sRBC exhibits a similar behaviour to the tRBC, but the membrane folding is not so obvious and the sRBC undergoes a tumbling motion. This is called breathing with tumbling motion (12).

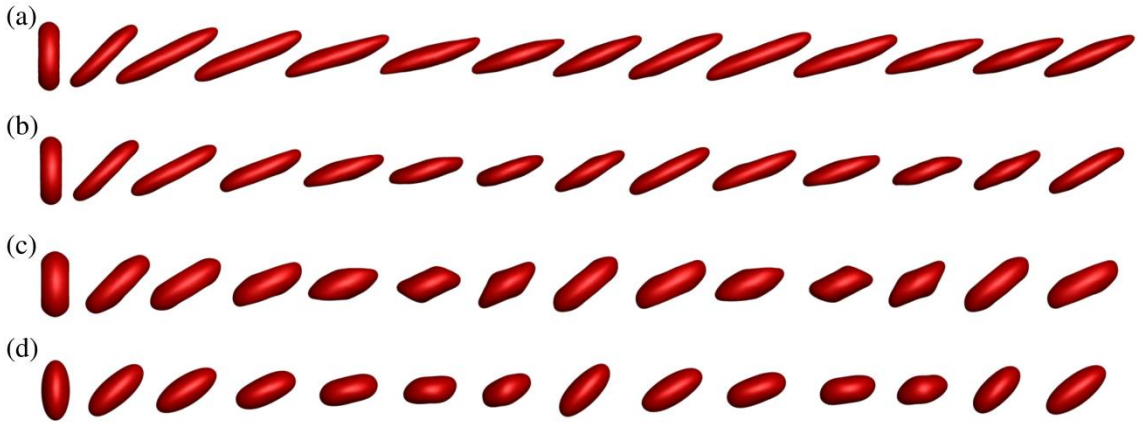

Fig. 1 Dynamic behaviours of (a) hRBC, (b) rRBC, (c) tRBC and (d) sRBC in simple shear flow with the shear rate $\dot{\gamma} = 1.7 \times 10^3 s^{-1}$. The snapshots are taken from 0 to 6.6 ms with the time interval of 0.508 ms.

References

1. Hoogerbrugge, P. J., and J. M. V. A. Koelman. 1992. Simulating Microscopic Hydrodynamic Phenomena with Dissipative Particle Dynamics. Europhys Lett 19:155-160.
2. Espanol, P., and P. Warren. 1995. Statistical-Mechanics of Dissipative Particle Dynamics. Europhys Lett 30:191-196.
3. Fedosov, D. A., B. Caswell, and G. E. Karniadakis. 2010. A multiscale red blood cell model with accurate mechanics, rheology, and dynamics. Biophys. J. 98:2215-2225.
4. Marko, J. F., and E. D. Siggia. 1995. Stretching DNA. Macromolecules 28:8759-8770.
5. Pozrikidis, C. 2003. Modeling and simulation of capsules and biological cells. Chapman & Hall/CRC, Boca Raton, FL.
6. Espanol, P. 1998. Fluid particle model. Phys Rev E 57:2930-2948.
7. Groot, R. D., and P. B. Warren. 1997. Dissipative particle dynamics: Bridging the gap between atomistic and mesoscopic simulation. J Chem Phys 107:4423-4435.
8. Suresh, S., J. Spatz, J. P. Mills, A. Micoulet, M. Dao, C. T. Lim, M. Beil, and T. Seufferlein. 2005. Connections between single-cell biomechanics and human disease states: gastrointestinal cancer and malaria. Acta Biomater 1:15-30.
9. Suresh, S. 2006. Mechanical response of human red blood cells in health and disease: Some structure-property-function relationships. J Mater Res 21:1871-1877.

10. Fedosov, D. A., B. Caswell, and G. E. Karniadakis. 2010. Systematic coarse-graining of spectrin-level red blood cell models. Comput Method Appl M 199:1937-1948.
11. Vlahovska, P. M., T. Podgorski, and C. Misbah. 2009. Vesicles and red blood cells in flow: From individual dynamics to rheology. Cr Phys 10:775-789.
12. Yazdani, A. Z. K., and P. Bagchi. 2011. Phase diagram and breathing dynamics of a single red blood cell and a biconcave capsule in dilute shear flow. Phys Rev E 84.